Front. Chem. Sci. Eng. 2021, 15(1): 187–197
https://doi.org/10.1007/s11705-020-1931-z

RESEARCH ARTICLE

Long-lasting photoluminescence quantum yield of cesium lead halide perovskite-type quantum dots

Yonghyun Kim[1], Huiwen Liu[2], Yi Liu[2], Boa Jin[1], Hao Zhang[2], Wenjing Tian (✉)[2], Chan Im (✉)[1]

1 Department of Chemistry, Konkuk University, Seoul 05029, Korea
2 State Key Laboratory of Supramolecular Structure and Materials, College of Chemistry, Jilin University, Changchun 130012, China

Abstract Cesium lead halide perovskite ($CsPbX_3$, X = Cl, Br, I) quantum dots (QDs) and their partly Mn^{2+}-substituted QDs ($CsPb_{1-x}Mn_xX_3$) attract considerable attention owing to their unique photoluminescence (PL) efficiencies. The two types of QDs, having different PL decay dynamics, needed to be further investigated in a form of aggregates to understand their solid-state-induced exciton dynamics in conjunction with their behaviors upon degradation to achieve practical applications of those promising QDs. However, thus far, these QDs have not been sufficiently investigated to obtain deep insights related to the long-term stability of their PL properties as aggregated solid-states. Therefore, in this study, we comparatively examined $CsPbX_3$- and $CsPb_{1-x}Mn_xX_3$-type QDs stocked for > 50 d under dark ambient conditions by using excitation wavelength-dependent PL quantum yield and time-resolved PL spectroscopy. These investigations were performed with powder samples in addition to solutions to determine the influence of the inter-QD interaction of the aged QD aggregates on their radiative decays. It turns out that the Mn^{2+}-substituted QDs exhibited long-lasting PL quantum efficiencies, while the unsubstituted $CsPbX_3$-type QDs exhibited a drastic reduction of their PL efficiencies. And the obtained PL traces were clearly sensitive to the sample status. This is discussed with the possible interaction depending on the size and distance of the QD aggregates.

Keywords quantum dots, cesium lead halide perovskite, time-resolved photoluminescence, PL quantum yield, QD aggregates

1 Introduction

Owing to the success of organic–inorganic hybrid perovskite materials as active photon absorbers in solar cells, perovskite materials have become one of the most important topics of study in various scientific communities [1–3]. Novel quantum dots (QDs) inspired by these perovskite structures have been synthesized. Some initial hybrid perovskite QDs exhibit moderate photoluminescence (PL) quantum yields (QYs) but with narrow full width at half maximum (FWHM) emission bands [4–6], which encourage further chemical tailoring of these perovskite QDs to improve their PL QYs and resolve their stability issues.

One of the most effective ways to design novel perovskite QDs is substitution of the organic components with a proper metal such as cesium. $CsPbX_3$ (X = Cl, Br, I) QDs exhibited improved stability [7–10] and an impressive PL efficiency with the use of, for example, $CsPbBr_3$ [11–13]. With the improved PL QYs of $CsPbX_3$ QDs, various groups have demonstrated their potential in light-emitting diodes [14–17], as well as lasing applications [18]. Furthermore, the optoelectronic properties of the QDs have been investigated for solar cells [19], photoelectric detectors [20], and specific metal-ion detection [21,22]. Those impressive results motivated further efforts for synthesis variations. For instance, Liu et al. showed that $CsPbX_3$-type QDs can be synthesized efficiently via a microwave irradiation method as a single-step reaction [23]. One of the QDs fabricated using this method exhibited a PL QY of > 90%. They also showed that the amount of toxic lead can be reduced while retaining the promising characteristics via replacement of lead with manganese. Some Mn^{2+}-substituted $CsPbX_3$-type QDs exhibit a high PL QY of approximately 50% but with a long spectroscopic lifetime [24]. It is noteworthy that there were studies to replace lead with other metals like bismuth or tin, but their PL QYs seem to be lower than that of

Received December 25, 2019; accepted March 3, 2020

E-mails: wjtian@jlu.edu.cn (Tian W); chanim@konkuk.ac.kr (Im C)

manganese case [25,26].

In most of the aforementioned studies, abundant information was obtained regarding the PL features, i.e., the PL emission spectra and PL QYs. In some studies, further spectroscopic results for those QDs were obtained by using the time-resolved PL and transient absorptions often in conjunction with their synthetic descriptions. Additional spectroscopic studies have been performed; for example, the temperature-dependent PL of QDs was measured to determine the PL characteristics of these promising materials [27,28]. PL studies have also been performed to investigate the stability issues by using the timely evolution of the PL properties for long time periods, as shown by Chen et al. [10]. However, more information must be gathered to understand in depth what exact exciton dynamics related to radiative decay occur within aged QD aggregates, particularly after long-term stocking under dark ambient conditions. Such information is crucial for precisely controlling these QDs to make them useful components for practical applications. Because it is advantageous to use the QDs in their solid-state form for most practical applications, the detailed radiative decay behaviors of the excitons within their solid phases, i.e., aggregates of QDs, compared with their corresponding liquid phases are essential. These behaviors also have scientific importance for depicting the complex exciton dynamics within disordered random QD solids governed by various energetic relaxation processes.

Therefore, we studied typical $CsPbX_3$-type QDs having a PL lifetime in the nanosecond range with a PL QY of approximately 90% before aging. For comparison, we also examined partly Mn^{2+}-substituted $CsPb_{1-x}Mn_xX_3$-type QDs having a significantly longer PL lifetime with a PL QY of approximately 50% before aging. The former and latter perovskite type QDs are denoted as perovskite QD1 (PQD1) and perovskite QD2 (PQD2), respectively. PQD1 and PQD2 were investigated using excitation wavelength-dependent steady-state PL QY and time-resolved PL spectroscopy. These spectroscopic investigations were performed with powder samples (PD) in addition to diluted (DS) and concentrated solutions (CS) to determine the influence of the sample phase, for example, the distance between QD aggregates and/or average QD aggregate size, on the exciton decay kinetics. The obtained results are presented with the following convention: the powder sample of PQD1 is denoted as PQD1-PD, for example.

After a stocking period longer than ~50 d under dark ambient conditions, for all sample phases, PQD1 exhibited a drastic reduction of the PL QY, whereas for PQD2, the PL QY was hardly reduced. Obviously, clear kinetic differences between the sample phases are confirmed, in addition to the dramatic steady-state PL QY difference between the two PQDs. These are discussed according to the distance between aggregates and the aggregate size for the QDs, which are important parameters for their solid-state application.

2 Experimental

PQD1 and PQD2 having experimentally estimated chemical compositions of $CsPbBr_{2.7}$ and $CsPb_{0.73}Mn_{0.27}Cl_3$ were synthesized at temperatures of 150°C and 170°C, respectively [23,24]. Their synthesis methods, including the feed ratios, and the characterization methods for verifying their compositions estimated via energy-dispersive X-ray spectroscopy and inductively coupled plasma spectroscopy are presented in detail in the aforementioned studies. The two PQDs were dispersed into a toluene solvent with concentrations of 4.3×10^{-5} wt-% (DS) and 4.3×10^{-4} wt-% (CS), respectively. In addition to those solutions, PQD powder samples — PQD1-PD and PQD2-PD — were measured using glass cells having an inner space length of approximately 0.3 mm.

Conventional steady-state ultraviolet-visible (UV-vis) absorption spectra were measured using a commercial two-beam spectrometer (NEOSYS-2000, Sinco, Korea). In addition, light integrating sphere-assisted steady-state UV-vis, PL, and PL excitation (PLE) spectra were measured by using a spectrometer (Quantaurus, Hamamatsu, Japan). The obtained data were used to estimate the PL QY as a function of the excitation wavelength. The spectrally resolved and time-resolved PL was recorded using a streak camera system (C13410, Hamamatsu, Japan) excited with an ultrashort-pulse laser system (Libra, Coherent, USA) followed by an optical parametric amplifier (TOPAS-C, Coherent, USA) to select a proper excitation wavelength. The excitation pulses were approximately 150 fs in length, and the pulse repetition rate was 1 kHz. The samples were mostly excited with a weak excitation intensity of approximately 0.3 $\mu W/cm^2$ to avoid the photon flux-dependent exciton–exciton interaction, which can shorten the native PL decay kinetics.

3 Results and discussion

In Fig. 1, three-dimensionally combined maps of the PL and PLE spectra for various samples of both PQD1 and PQD2 are shown. The combined PL and PLE spectra were measured using a light integrating sphere-equipped spectrometer in order to reduce the QD aggregate-induced scattering effects. As shown in Figs. 1(a) and 1(d), PQD1-DS has a PL band centered at 521 nm, while PQD2-DS has two bands centered at 408 and 600 nm, although the band centered at 404 nm is significantly shallower and weaker than that at 600 nm. The FWHM is ~100 meV for the band at 404 nm, ~300 meV for the other band at 600 nm, and ~90 meV for PQD1-DS. The band centered at 404 nm can be the mutual emission band of the $CsPbX_3$-type QDs without Mn^{2+} substitution, as previously reported [24]. The disappearance of the band at 404 nm of PQD2-PD as shown in Fig. 1(f) in conjunction with the weakening of the

same band as shown in Figs. 1(d) and 1(e) will be further analysed with corresponding kinetic results at the end of the discussion part.

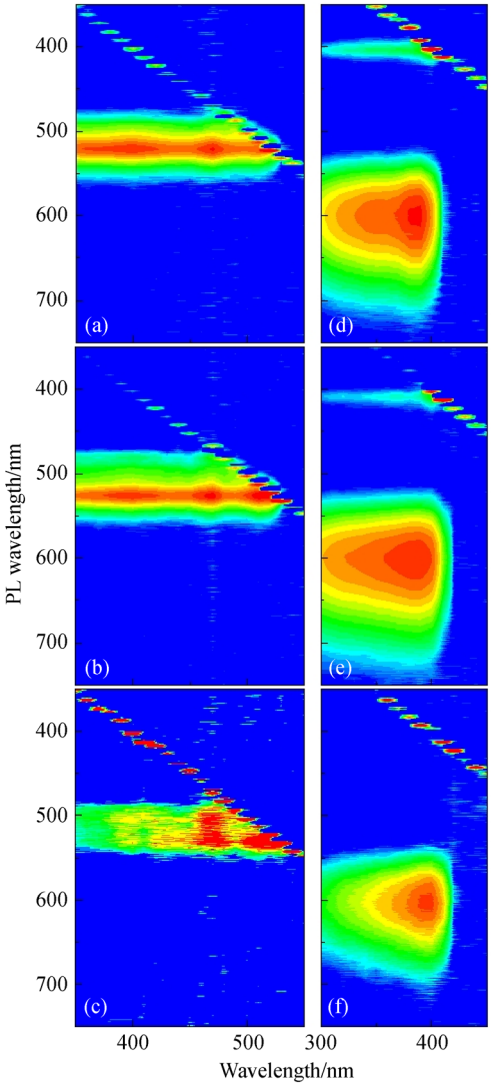

Fig. 1 Three-dimensional mappings of the combined PL and PLE spectra of (a) DS, (b) CS, and (c) PD of PQD1 and of (d) DS, (e) CS, and (f) PD of PQD2.

Compared with the previously reported PL peak position of PQD1 (517 nm with an FWHM of ~80 eV), all the aged PQD1 samples exhibited only a marginal redshift, but their FWHMs were significantly broadened [23]. The PL QY of the fresh PQD1 sample was 90%, and that of the aged sample was reduced by almost an order of magnitude. Most of the aged PQD2 samples had two PL bands, in accordance with the fresh samples. However, their peak values were significantly redshifted after aging, from 390 and 579 nm to ~404 and 600 nm, respectively, in all sample conditions, whereas the shifts of PQD1 were only marginal [24]. A unique result of aged PQD2-PD was that their PL QY values were virtually identical to that of the corresponding fresh sample with the value of 54%. All the important steady-state PL parameters estimated in this study are presented in Table 1.

With the change of the solution concentration, the central positions of the PL bands for PQD1 were only marginally redshifted, from 521 nm for PQD1-DS in Fig. 1(a) to 526 nm for PQD1-CS in Fig. 1(b). However, the PL band for PQD1 appeared to be split into two bands when the samples were solidified to PQD1-PD from PQD1-DS and PQD1-CS. The bands were centered at 499 and 529 nm, and the difference between the split bands was approximately 130 meV. Interestingly, the PQD2 samples centered at ~600 nm did not exhibit any significant spectral shifts between PQD2-DS, PQD2-CS, and PQD2-PD, as shown in Figs. 1(d–f), respectively. However, the bands centered near 400 nm were clearly reduced by increasing the concentration of the solutions and almost disappeared when the PQD2 was measured in the form of powder.

The PLE trends for PQD2 appeared to be affected by the concentration and the phase change of the samples. This strongly indicates that the exciton dynamics were mostly governed by the energetic relaxation, which depended on the interaction between QDs controlled by their distances and sizes. For that, schematics of the three investigated sample phases are shown in Fig. 2. In the DS samples, the QD aggregates with typical sizes on the order of 10 nm can be well-dispersed even with relatively small aggregate sizes, as shown in Fig. 2(a), while in the CS samples, the aggregate sizes may increase, and the average distances

Table 1 Steady-state PL results

QD	Sample phase	$1^{st}\lambda_{max}$ [FWHM] [a]	$2^{nd}\lambda_{max}$ [FWHM]	$\Delta\lambda_{max1,2}$ [c]	PL QY [d] aged /%	PL QY fresh /%
PQD1	DS	521 [100]	(494) [b] [130]	(130)	9.1	90 (cf. [23])
	CS	526 [90]	(493) [130]	(130)	3.0	
	PD	529 [150]	499 [150]	130	6.3	
PQD2	DS	600 [300]	404 [110]	990	22.6	
	CS	600 [300]	408 [120]	960	28.1	54 (cf. [24])
	PD	600 [300]	–	–	49.3	

a) The values of FWHM are listed with rectangular brackets in meV; b) The values in round brackets are used to indicate relatively high uncertainty due to weak signals; c) The $\Delta\lambda_{max1,2}$ stands for the difference between "$1^{st}\lambda_{max}$" and "$2^{nd}\lambda_{max}$" of PL bands in meV; d) The values of PL QY are taken at 450 nm for PQD1 and 380 nm for PQD2; All λ_{max} values are listed in nanometer and FWHM values are listed in meV.

between aggregates must be smaller, as shown in Fig. 2(b). Therefore, transitional behaviors can be observed with the CS positioned between well-dispersed QDs in the DS, showing the pronounced native properties of the PL and the aggregation-dominant PD being governed by pronounced diffusive exciton dynamics, as depicted in Fig. 2(c).

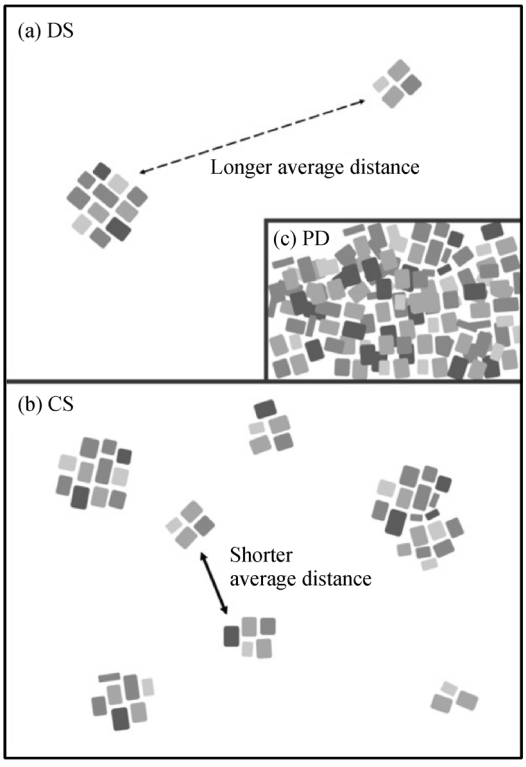

Fig. 2 Schematics of the (a) DS, (b) CS, and (c) PD QD samples.

As mentioned previously, native QDs with nanoscale sizes and their aggregates with even larger sizes may have serious scattering effects, which can cause overestimation compared with their mutual photon absorption facility under a measurement condition without light integrating equipment. For example, the UV-vis absorption spectrum of PQD1-DS measured using a conventional two-beam spectrometer is shown in Fig. 3(a). The spectrum is compared with a fitting curve based on a $1/\lambda^4$ functionality (λ = wavelength) because the intensity of Rayleigh scattering is proportional to the $1/\lambda^4$ term. As expected, the fitting curve exhibits the same trend as the experimentally estimated UV-vis spectrum without a light integrating sphere, because the scattered light amount is regarded as the absorbed light amount in such a situation.

The absorption spectra of the DSs shown in Fig. 3(b) were measured using a light integrating sphere; hence, they exhibit a reduced scattering feature compared with the conventional spectrum shown in Fig. 3(a), especially in the

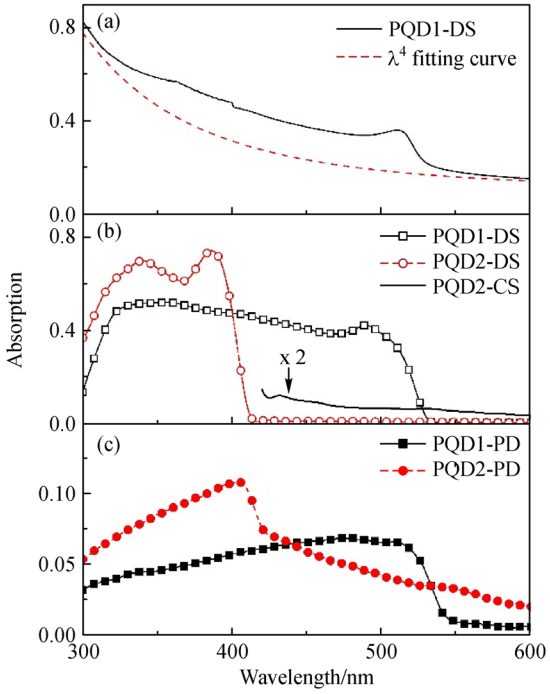

Fig. 3 UV-vis absorption spectra of (a) a PQD1 dilute solution measured with a two-beam spectrometer, as well as (b) solutions and (c) powders measured with an integrating sphere.

short-wavelength range. Similarly, the spectra of the PDs in Fig. 3(c), which were also measured using a light integrating sphere, exhibit a significantly reduced scattering effect. It must be noticed that the absorption term used in this study including Fig. 3 is not for the conventional absorbance but for the absorption expressed in fraction numbers to keep consistency with PL QY convention. Surprisingly, the PQD2-PD spectrum indicates significant absorption in the long-wavelength range starting from 420 nm, while the PQD2-DS spectrum indicates no significant absorption in the same spectral range, as shown in Fig. 3(b). However, the PQD2-CS spectrum contains an absorption feature in this spectral range, as shown in Fig. 3(b) (straight-lined spectrum multiplied by a factor of 2 for better readability). The PQD2-DS has a similar absorption feature in the spectral range, but the magnitude is too low to observe this clearly in the linear scale plot, as shown in Fig. 3(b). The absorption feature appears sudden and non-linear owing to the solidification due to the intrinsic optical property of PQD2, regardless of the aggregation degree. This is attributed to the incomplete substitution of Mn^{2+} with Pb^{2+}, and the weak absorption in the long-wavelength range is attributed to the Pb^{2+}-rich domains. The reason why these weakly absorbing parts are more pronounced in aged solid samples might be related to the phase separation between Mn^{2+} and Pb^{2+}, resulting in Mn^{2+}- and Pb^{2+}-rich domains after long-term aging. It is

plausible that the Mn^{2+}-rich domains undergo serious structural change compared with the Pb^{2+}-rich domains. This scenario is supported by the notion that excessive substitution of Mn^{2+} can cause severe changes in the perovskite structure [24].

The absorption values for the PD samples (PQD maxima of ~0.05 and ~0.1 for PQD1 and PQD2, respectively) were significantly smaller than those for the DS samples (~0.5 and ~0.7, respectively). The reason for the low absorption values of the PD samples was that a small amount of the PD samples was used for the measurement in order to avoid complications due to the multiple stacking of QDs, e.g., saturation and/or self-reabsorption caused by the formation of excessively thick aggregates or QD layers.

As shown in Figs. 4(a–c), PQD1 exhibited clear aggregation degree-dependent features, in addition to an aging effect indicated by a redshift, the broadening of the FWHM, and the enhancement of the secondary PL band. The important values extracted from Fig. 4 are presented in Table 1. The excitation wavelength-dependent PL spectra of PQD1-DS remained virtually unchanged, while those of PQD1-CS exhibited a moderate redshift of the PL maxima, from 521 to 526 nm. The increase of the secondary PL band near 493 nm, which was energetically higher than the mutual PL band, became more pronounced with the decrease of the excitation wavelength. As expected, the secondary QD aggregation-induced PL bands were more pronounced for the PD sample than those of DS and CS samples. These secondary PL bands of PQD1-PD increased and simultaneously were broadened with the decrease of the excitation wavelength, which can indicate pronounced disorder caused by the aging of the QD aggregates. The pronounced secondary peak of PQD1-PD is very close to the PL peak value of fresh PQD1, which was previously reported as 508 nm [23].

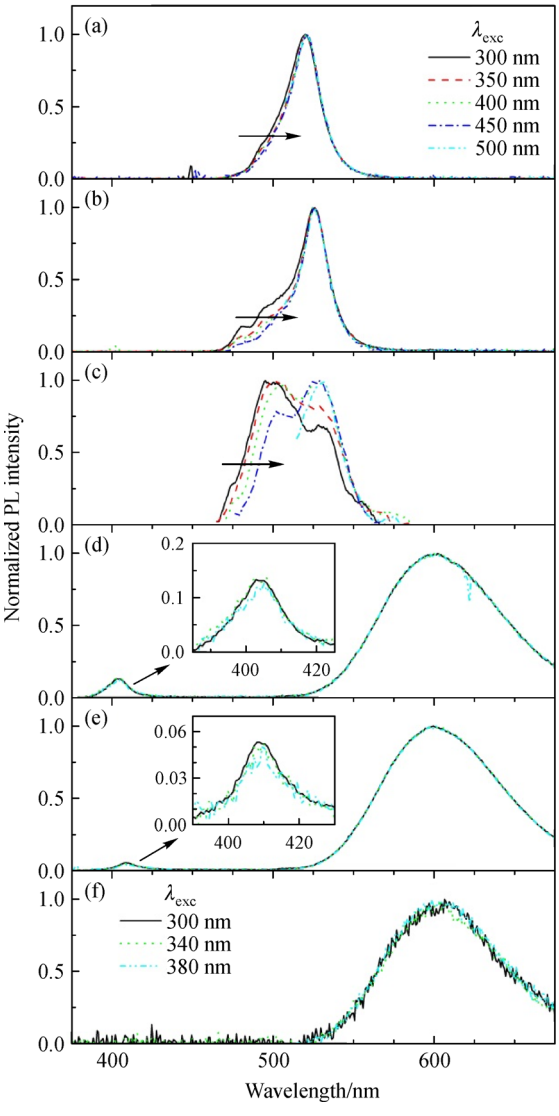

Fig. 4 Excitation wavelength-dependent PL spectra of various PQD samples. The legend in (a) also applies to (b) and (c), and that in (f) also applies to (d) and (e).

The FWHM of the PL band for PQD1-DS was approximately 100 meV, and that for PQD1-CS was approximately 90 meV. However, the FWHMs in both the primary and secondary PQD1-PD cases appeared to be significantly extended to approximately 150 meV, indicating an enhanced disorder effect. An additional unique feature related to the FWHMs is that PQD2 had a significantly broad FWHM of PL bands centered at 600 nm, with a value of approximately 300 meV. The major PL bands of the PQD2 samples were the same regardless of whether the samples were dispersed in a liquid solution or solidified as powder, indicating that the emission is a native QD property unaffected by aggregation. However, the small PL bands near 400 nm, which appear only in the solution steady-state PL spectra, have FWHMs of 110–120 meV, similar to the primary PL bands for the PQD1 solutions. This is evidence that the origin of the small bands was non-substituted PQDs, although their peak intensity was dramatically reduced after aging compared with the corresponding fresh samples. However, the small PL bands near 400 nm for PQD2 did not significantly change in intensity, spectral maximum peak position, or FWHM with the change of the excitation wavelength.

The PL bands in conjunction with the corresponding UV-vis absorption spectra shown in Fig. 3 reveal the following. For PQD1, the PL bands centered between 493 and 529 nm are mostly covered by the UV-vis spectral range, because the edge of the UV-vis absorption is approximately 540 nm after aging, in accordance with a previous report [10]. This must enhance the self-reabsorption of the PL emission, which is an additional reason why PQD1 had a lower PL QY than fresh PQD1 after aging. However, the PQD2 samples were less affected by the aging because PQD2 had enough distance between the absorption and emission bands to avoid serious self-reabsorption. The pronounced redshift of the absorption

edge and hence the intense overlapping between the PL and UV-vis spectra are correlated with the generation of energetically lower bands after aging. These new aging-induced bands must be correlated with the newly generated defect sites (DeS), in addition to the enlargement of the aggregates, accompanied by the redshift trend with the increase of the QD concentration of the samples.

Although the energetically lower band of PQD2 exhibits no pronounced overlapping between the absorption and emission bands, the small PL bands of PQD2 centered near 400 nm have a strong adjacent absorption band centered around 390 nm, which can cause effective overlapping, as in the case of PQD1. This allows highly effective energy and/or electron transfer from the secondary band to DeSs generated during aging, as in the PQD1 systems. The maximum peak heights of the secondary small bands of PQD2-DS are approximately 13% relative to the primary bands, while those for PQD2-CS are only approximately 5%, and the values are significantly smaller than those of the fresh samples. This is strong evidence of pronounced DeS-induced dissipation during the exciton relaxation within the density of states (DOS) of PQD2-PD. Notably, the aggregation of PD does not cause the serious redshift typical for molecular organic semiconducting materials, which might be an additional advantage of these QD materials.

According to the obtained UV–vis absorption spectra and the corresponding PLE spectra, the spectrally resolved PL QY values were estimated, as shown in Fig. 5. All the PQD samples exhibit a well-established plateau region in the PL QY spectra. The PL QY spectra have homogenously scalable dependences; therefore, with multiplication by the proper scaling factors, the PL QY plots overlap each other without any significant deviations. This scalability indicates that the frameworks of the exciton decays for the various samples are consistent within the parametric adjustability. The scalability also indicates the acceptable reproducibility of the PL QY estimation method used in this study. However, the slight increasing trend with the decrease of the wavelength regardless of the sample conditions may indicate that there are inadvertent external influences on the estimation of the PL QY spectra. One of the most interesting observations from the PL QY after long-term aging is that all the PQD2 samples have significantly higher PL QYs than the PQD1 samples. The PL QYs of PQD1 estimated with fresh samples are significantly higher than those of the PQD2 samples, because the PL QY of PQD2 is almost constant, while that of PQD1 decreases dramatically after long-term aging from ~90% to ~10% levels. The PL QY of PQD2-DS was reduced by approximately 50% compared with the fresh sample, but the solid PQD2-PD retained the PL QY of the fresh sample. This implies that the closely packed aggregates had ways to re-populate toward the main emission band.

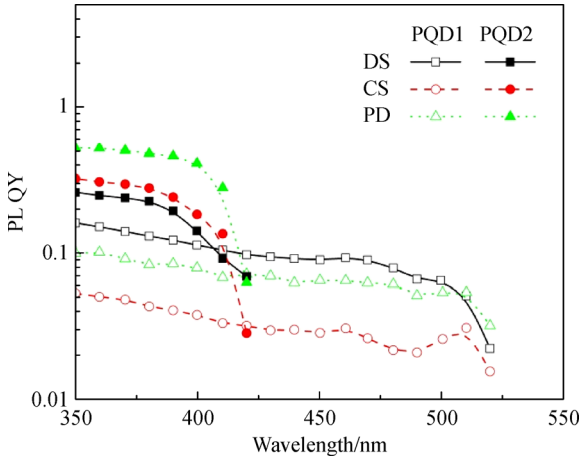

Fig. 5 PL QY spectra of PQD1 and PQD2 samples based on PLE spectra with 20 nm interval between excitation wavelengths.

PQD1-DS shows the highest PL QY values among the various PQD1 samples; they are more than two times higher than those of PQD1-CS and approximately 50% higher than those of PQD1-PD when compared at the plateau levels. Interestingly, the PL QYs of PQD2-DS are the lowest among all the PQD2 samples. The PL QY values of PQD2-CS are slightly higher than those of PQD2-DS, and PQD2-PD has PL QYs almost two times higher than those of PQD2-DS. The results indicate that PQD2 has more pronounced PL emission efficiency with increasing inter-QD interaction than PQD1, even after aging. The reduction of the PL QYs from DS to CS and the transformation of the solution to a solid are common features related to the PL, except for some aggregation-induced emission-facilitated materials [29]. This is evidence that the behaviors of excitons within these QD materials are complex and their decay pathways need to be explored using time-resolved spectroscopy as follows.

Figure 6 shows the time-resolved PL spectra of PQD1-CS and PQD1-PD samples. The excitation wavelengths for all the time-resolved PL measurements in this study were kept at 350 nm for comparison between the kinetics of the PQD1 and PQD2 samples, as PQD2 has a pronounced absorption band located significantly below 400 nm, as shown in Fig. 3. Obviously, PQD1-PD exhibited a more enhanced spectral relaxation feature than PQD1-CS. This implies that the excitons generated within the solid phase of PQD1-PD had improved energetic downhill migration within the lifetime window compared with their solution samples of PQD1. The transient spectrum of PQD1-DS is not shown, because it is practically the same as that of PQD1-CS, despite the lower QD concentration.

As shown in Fig. 6, the lifetime of PQD1-CS appears shorter than that of PQD1-PD. However, the emission band of PQD1-PD appears to be slightly blue-shifted compared with that of PQD1-CS, as shown in Fig. 4. The blue-shift of a PL band is often correlated with the shortening of the lifetime caused by the increase of defect

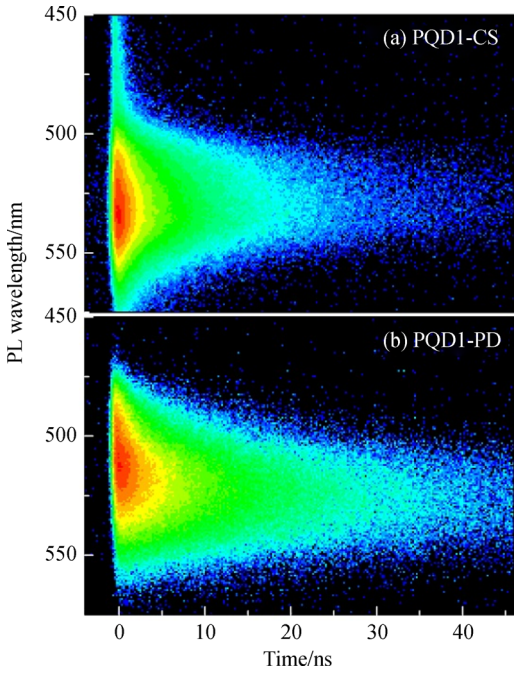

Fig. 6 Time-resolved PL spectra of (a) PQD1-CS and (b) PQD1-PD with excitation wavelength of 350 nm.

or trap states generated during aging, which can accelerate the depopulation of excitons before they can relax toward energetically lower sites within the DOS for subsequent radiative recombination which can be observed in randomly disordered polymeric solid systems [30]. In Fig. 7, time-dependent slices of the PL band for PQD1-PD taken from Fig. 6(b) are shown for clear quantitative evaluation of the spectral relaxation feature with the PQD1-PD solid system with the plot of peak positions as a function of time in the inset of Fig. 7 also. The spectroscopic lifetime of PQD1-PD appears to be significantly longer than that of PQD1-CS, although the higher-energy part of the PQD1-PD PL band is significantly blue-shifted, while the lower-energy part appears to be marginally redshifted. This is indicated by the extended FWHM with the splitting of the steady-state PL band feature, as shown in Fig. 4. Nevertheless, the extended PL lifetime of PQD1-PD provides a consistent result in accordance with the steady-state PL QY: the PQD1-PD solid has a higher PL QY than the PQD1-CS, as shown in Fig. 5. Interestingly, this increase of the PL QY with the formation of aggregates appears to be similar to that for the PQD2 system at least partly.

Figure 8 shows the time-resolved PL kinetics of PQD1 samples extracted near the PL band maxima. Most of the PL kinetic traces for the aged PQD1 samples have two distinctive regions: a rapidly decaying prompt part and a slowly decaying longer tail part. As an exception, the PL bands of PQD2 at ~600 nm have extremely long mono-exponentially decaying lifetimes of ~0.55 ms. Figures ESM-1 and ESM-2 in the Electronic Supplementary Materials show the time-resolved PL spectra of PQD2-CS and PQD2-PD, respectively. The obtained kinetics of PQD2 were possibly affected by the accumulation effect at a pulse repetition rate of 1 kHz, which is equivalent to a laser pulse-to-pulse interval time of 1 ms, although the excitation intensity was kept as low as possible. All the kinetic parameters extracted as biexponential decay functions are presented in Table 2, except for the main PL band kinetics for PQD2. Actually, a mono-exponential decay pattern is typical for a DS of a molecular compound because no significant exciton migration and/or electron transfer are expected; hence, the PL decay is governed by a mono-exponential functionality when there is only a sort of optically active functional group being dispersed with enough separation between them preventing a strong

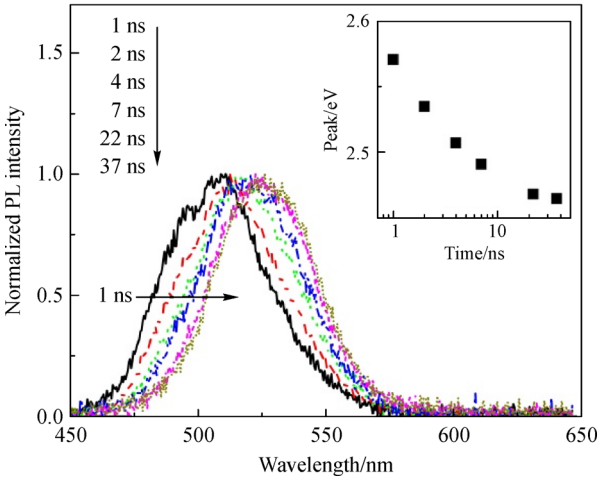

Fig. 7 Time-resolved slices of the PL band for PQD1-PD shown in Fig. 6(b). A plot of the peak positions in eV scale of the PL slices as a function of time is shown in the inset.

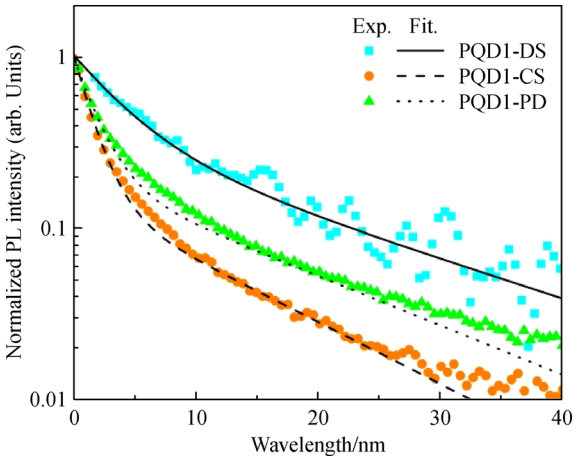

Fig. 8 Time-resolved PL decay kinetics of (a) PQD1-DS, (b) PQD1-CS, and (c) PQD1-PD.

interaction. Nevertheless, PQD1-DS shows a biexponential decay pattern with significantly weaker initial rapid decay than the higher-QD concentration solution. This means that the aggregation of aged PQD1 stimulates the efficient depopulation of primary excitons, reducing the PL QY.

Although most of the kinetic traces in Fig. 8 were satisfactorily fitted with biexponential functions, as indicated by the fitting lines in Fig. 8, the decay patterns of PQD1-CS and PQD1-PD exhibit also slight deviation from a biexponential pattern. This deviation can be compared with a stretched exponential pattern based on the spectral relaxation feature as shown in Fig. 7, while the deviation with PQD1-DS is negligible. And this indicates that the diffusion-controlled spectral relaxation plays a role in the decay of excited species within those disordered QD aggregates of PQD1-CS and PQD1-PD. Thus, it could be suggested that PQD1-DS has mainly one dominant PL active site in a less disordered QD aggregate, at least during a single-pulse process. However, a larger QD aggregate can undergo DeS-induced quenching or electron transfer to dissipate non-radiatively with a higher probability than well-dispersed individual QD aggregates. Of course, this feature becomes more important when the average inter-QD distances decrease from DS to CS or PD. This consideration may explain why the promptly decaying lifetime, $\tau 1$, becomes shorter in the case of PQD1 changing from DS to CS or PD. However, an efficient repopulation channel can be established by gathering more QD aggregates during solidification; therefore, the lifetime of the powder samples can be extended slightly. This hypothetical suggestion might be a plausible reason why the PL QYs of the PQD1 samples decrease in the order of PQD1-DS > PQD1-PD > PQD1-CS. This initial suggestion for the complicated behavior of PQD1 samples will be sumarized after the consideration about the PQD2 system with a schematic of the radiative decay paths as shown in Fig. 9 again.

In a previous study [24], fresh PQD1 samples without Mn^{2+} substitution exhibited a lifetime of about 10 ns, which is significantly longer than the lifetime of < 4 ns measured at the prompt parts of the aged samples. The reduction of the decay lifetime at the initial stage after aging indicates that the fresh samples had less DeSs and hence a significantly higher PL QY than the long-term aged samples. Chen et al. reported the effects of aging on

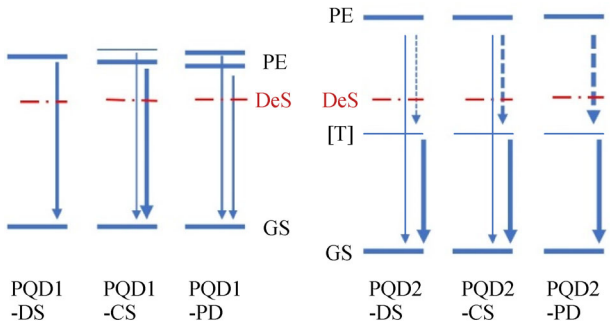

Fig. 9 Schematic of the radiative decay paths.

the PL properties of $CsPbBr_3$ and found that the PL peak of a fresh sample centered at ~503 nm was significantly redshifted to ~517 nm after aging under illumination for 6 d [10]. In addition, they reported that the PL intensities were drastically reduced after aging under illumination, accompanied by a clear redshift, whereas the aging effect without illumination was observable but significantly slower than that under illumination. Chen et al. extracted the lifetimes for the initial decay of approximately 4.2 ns and a longer decay of approximately 43.5 ns, which are comparable to the values obtained in this study, as shown in Table 2.

The kinetic behaviors of PQD2 appear to be drastically different from those of PQD1 because the lifetime of the band at ~400 nm is one order of magnitude shorter than that for PQD1, while the lifetime of the band at ~600 nm is more than one order of magnitude longer than that for PQD1. Therefore, the band at ~600 nm was assigned as the triplet emission band in a previous study [24]. Interestingly, all the PL bands of PQD2 have no significant spectral relaxation regardless of the sample states, as there are no spectral shift features in their steady-state PL results, as shown in Fig. 4. Liu et al. reported that Mn^{2+}-substituted PQD2 exhibited a short lifetime of 13.4 ns for the higher small band and a longer lifetime of approximately 1.6 ms for the lower main band with a fresh sample [24]. The short lifetimes for the higher bands of the aged PQD2 samples were shortened by approximately two orders of magnitudes, while the long lifetimes of the aged PQD2 samples were shortened to only approximately 1/3 after aging compared with the native lifetime estimated with a fresh sample. As a consequence, a weak PL peak at ~400 nm of

Table 2 Time-resolved PL fitting results

QD	Phase	$\tau 1$	$\tau 2$	A1	A2
PQD1	DS	4.0	19	0.70	0.33
	CS	1.5	12	0.88	0.15
	PD	1.8	15	0.80	0.20
PQD2	DS	0.082	0.55	0.85	0.15
	CS	0.12	1.0	0.86	0.14

PQD2-PD sample could be detected only with fast time-resolved PL measurement, which was not detectable in the steady-state PL spectra as shown in Fig. 1 and Fig. 4. However, the PL decay of this band was too fast to extract the reliable spectroscopic lifetime with the measurement setup used in this study. This means that the initial decay being accelerated by aging-caused species must be significantly enhanced compared with those of the solution samples; thus, the extremely short lifetime of PQD2-PD could not be presented in Table 2. Despite the drastic change of the PL kinetics in particular regarding the small band at ~400 nm, the PL QY of a solid PQD2-PD sample was not seriously reduced from the value of a fresh sample. This let us assum that there is a kind of repopulation pathway toward strong emissive band at 600 nm after pronounced depopulation which compete with the emission of small band at ~400 nm.

In Fig. 9, the decay paths and assignments for relevant excited species are schematically presented. The DeS generated during the aging process can be responsible for the efficient non-radiative depopulation of the PEs of both PQD1 and PQD2, as discussed in relation to the shortening of the initial lifetimes (τ1 in Table 2). However, for PQD1, there are only few states below the energy level of DeS that can stimulate the repopulation of such trapped excitons toward radiative species, whereas for PQD2, there are triplet levels having a high population probability below the DeS that can still effectively undergo phosphorescence or delayed fluorescence. Therefore, the aging-induced DeS plays the role of a quencher for PQD1, whereas it does not for PQD2. Furthermore, the extremely efficient migration to the DeS might be beneficial to the subsequent population toward the triplet states; thus, the PL QY order of PQD2-DS < PQD2-CS ≪ PQD2-PD for PQD2 samples can be explained by the above postulate.

Comparing of the PQD1 and PQD2 systems by means of their schematic decay pathways as shown in Fig. 9 can give an answer for the question regarding the lifetimes of the solid systems being longer than those of the solution systems, followed by short initial decaying lifetimes of the PQD1 system. The aforementioned postulate may support the notion that the strongly interacting PD system has additional ways to re-populate toward a mutual emitting state — probably primary excitons via one or more transitional states, such as triplet, charge transfer states [31], or even free charge carrier states. Both PQD1 and PQD2 have very effective PE migration after DeS generation during aging processes but with different consequences owing to the different mechanisms after the first depopulation of PE. For instance, PQD2 has a significantly longer emission regardless of the aging or sample conditions, indicating its high intrinsic inter-system crossing probability due to Mn^{2+} substitution. This makes the PL QY changes upon aging completely different between the two systems — PQD1 and PQD2. In addition to the effect of this intrinsic difference, the disordered aggregation degree-dependent effect plays an important role in determining the excitonic fates. The changing of the fluorescence lifetime is triggered by not only the reduction of the inter-QD distances due to the higher concentration but also the formation of larger QD aggregates, as triplet transfer must be governed by a short-range interaction such as Dexter transfer and cannot easily occur via a Förster-type mechanism. Another hypothetical scenario is as follows: plenty of long-living triplet excitons within a solid of larger QD aggregates can extend the probability of triplet-triplet annihilation-induced delayed fluorescence [32] which need to be further studied.

4 Conclusions

Aged cesium lead halide perovskite QDs and their Mn^{2+}-substituted QD counterparts ($CsPbBr_{2.7}$ and $CsPb_{0.73}Mn_{0.27}Cl_3$, which are denoted as PQD1 and PQD2, respectively) were investigated via excitation wavelength-dependent PL QY and time-resolved PL spectroscopy. The measurements were performed using DS, CS and PD QD samples kept under ambient conditions for a long-term period of approximately two months.

After long-term stocking-induced aging, PQD1 exhibited a drastically reduced PL QY, whereas the PL QY of PQD2 was almost unchanged. The aging-induced defects of PQD1 were extremely effective for enhancing the relaxation via non-radiative decay pathways. The PL QY of PQD2 was not affected by the aging-induced defects, although PQD2 had a comparable effect due to aging-induced defects, as indicated by the energetically higher PL band. A comparison of the phase situations of the different samples revealed clearly different exciton interactions.

As expected, the non-radiative decay of PQD1 was enhanced by the reduction of the distances between QD aggregates from CS to DS and PD, whereas that of PQD2 was prohibited by the reduction of the distances between QD aggregates. Notably, the distance between the QD aggregates is an important parameter determining the solid-state application of the material. Obviously, the differences between PQD1 and PQD2 with regard to the position of DeSs in their decay path schema and the exciton diffusion caused by close packing in the solid-state sample give PQD2 a significantly longer-lasting PL, which is crucial for light-emitting applications under extreme environmental conditions.

Acknowledgements This work was supported by the research program of Konkuk University in 2018.

Electronic Supplementary Material Supplementary material is available in the online version of this article at https://doi.org/10.1007/s11705-020-1931-z and is accessible for authorized users.

References

1. Yang W S, Noh J H, Jeon N J, Kim Y C, Ryu S, Seo J, Seok S. High-performance photovoltaic perovskite layers fabricated through intramolecular exchange. Science, 2015, 348(6240): 1234–1237
2. Saliba M, Matsui T, Seo J Y, Domanski K, Correa J P, Nazeeruddin M K, Zakeeruddin S M, Tress W, Abate A, Hagfeldt A, et al. Cesium-containing triple cation perovskite solar cells: Improved stability, reproducibility and high efficiency. Energy & Environmental Science, 2016, 9(6): 1989–1997
3. Chen W, Bao X, Zhu Q, Zhu D, Qiu M, Sun M, Yang R. Simple planar perovskite solar cells with a dopant-free benzodithiophene conjugated polymer as hole transporting material. Journal of Materials Chemistry. C, Materials for Optical and Electronic Devices, 2015, 3(39): 10070–10073
4. Pan J, Quan L N, Zhao Y, Peng W, Murali B, Sarmah S P, Yuan M, Sinatra L, Alyami N M, Liu J, et al. Highly efficient perovskite-QD LEDs by surface engineering. Advanced Materials, 2016, 28: 8718–8725
5. Tan Z K, Moghaddam R S, Lai M L, Docampo P, Higler R, Deschler F, Price M, Sadhanala A, Pazos L M, Credgington D, et al. Bright LEDs based on organometal halide perovskite. Nature Nanotechnology, 2014, 9(9): 687–692
6. Yoon H C, Kang H, Lee S, Oh J H, Yang H, Do Y R. Study of perovskite quantum dot down-converted LEDs and six-color white LEDs for future displays with excellent color performance. ACS Applied Materials & Interfaces, 2016, 8(28): 18189–18200
7. Swarnkar A, Chulliyil R, Ravi V K, Irfanullah M, Chowdhury A, Nag A. Colloidal $CsPbBr_3$ perovskite nanocrystals: Luminescence beyond traditional quantum dots. Angewandte Chemie International Edition, 2015, 54(51): 15424–15428
8. Tong Y, Bladt E, Aygüler M F, Manzi A, Milowska K Z, Hintermayr V A, Docampo P, Bals S, Urban A S, Polavarapu L, Feldmann J. Highly luminescent cesium lead halide perovskite nanocrystals with tunable composition and thickness by ultrasonication. Angewandte Chemie International Edition, 2016, 55(44): 13887–13892
9. Kulbak M, Cahen D, Hodes G. How important is the organic part of lead halide perovskite photovoltaic cells? efficient $CsPbBr_3$ cells. Journal of Physical Chemistry Letters, 2015, 6(13): 2452–2456
10. Chen J, Liu D, Al-Marri M J, Nuuttila L, Lehtivuori H, Zheng K. Photo-stability of $CsPbBr_3$ perovskite Quantum Dots for optoelectronic application. Science China Materials, 2016, 59(9): 719–727
11. Akkerman Q A, Motti S G, Srimath Kandada A R, Mosconi E, D'Innocenzo V, Bertoni G, Marras S, Kamino B A, Miranda L, de Angelis F D, Petrozza A, Prato M, Manna L. Solution synthesis approach to colloidal cesium lead halide perovskite nanoplatelets with monolayer-level thickness control. Journal of the American Chemical Society, 2016, 138(3): 1010–1016
12. Akkerman Q A, D'Innocenzo V, Accornero S, Scarpellini A, Petrozza A, Prato M, Manna L. Tuning the optical properties of cesium lead halide perovskite nanocrystals by anion exchange reactions. Journal of the American Chemical Society, 2015, 137 (32): 10276–10281
13. Li X, Cao F, Yu D, Chen J, Sun Z, Shen Y, Zhu Y, Wang L, Wei Y, Wu Y, Zeng H. All inorganic halide perovskites nanosystem: Synthesis, structural features, optical properties and optoelectronic applications. Small, 2017, 13(9): 1603996
14. Chen W, Xin X, Zang Z, Tang X, Li C, Hu W, Zhou M, Du J. Tunable photoluminescence of $CsPbBr_3$ perovskite quantum dots for light emitting diodes application. Journal of Solid State Chemistry, 2017, 255: 115–120
15. Wang H C, Bao Z, Tsai H Y, Tang A C, Liu R S. Perovskite quantum dots and their application in LEDs. Small, 2018, 14(1): 1702433
16. Song P, Qiao B, Song D, Liang Z, Gao D, Cao J, Shen Z, Xu Z, Zhao S. Colour- and structure-stable $CsPbBr_3$-$CsPb_2Br_5$ compounded Quantum Dots with tuneable blue and green light emission. Journal of Alloys and Compounds, 2018, 767: 98–105
17. Zhang X, Wang W, Xu B, Liu S, Dai H, Bian D, Chen S, Wang K, Sun X W. Thin film perovskite LED based on $CsPbBr_3$ powders and interfacial engineering. Nano Energy, 2017, 37: 40–45
18. Li J, Dong H, Xu B, Zhang S, Cai Z, Wang J, Zhang L. $CsPbBr_3$ perovskite Quantum Dots: Saturable absorption properties and passively Q-switched visible lasers. Photonics Research, 2017, 5(5): 457–460
19. Chen L C, Lee K L, Huang C Y, Lin J C, Tseng Z L. Preparation and characteristics of $MAPbBr_3$ perovskite quantum dots on NiO_x film and application for high transparent solar cells. Micromachines, 2018, 9(5): 205
20. Liu D, Hu Z, Hu W, Wangyang P, Yu K, Wen M, Zu Z, Liu J, Wang M, Chen W, Zhou M, Tang X, Zang Z. Two-step method for preparing all-inorganic $CsPbBr_3$ perovskite film and its photoelectric detection application. Materials Letters, 2017, 186: 243–246
21. Sheng X, Liu Y, Wang Y, Li Y, Wang X, Wang X, Dai Z, Bao J, Xu X. Cesium lead halide perovskite quantum dots as a PL probe for metal ions. Advanced Materials, 2017, 29(37): 1700150
22. Liu Y, Tang X, Zhu T, Deng M, Ikechukwu I P, Huang W, Yin G, Bai Y, Qu D, Huang X, Qiu F. All-inorganic $CsPbBr_3$ perovskite Quantum Dots as a PL probe for ultrasensitive Cu^{2+} detection. Journal of Materials Chemistry. C, Materials for Optical and Electronic Devices, 2018, 6(17): 4793–4799
23. Liu H, Wu Z, Gao H, Shao J, Zou H, Yao D, Liu Y, Zhang H, Yang B. One-step preparation of cesium lead halide $CsPbX_3$ (X = Cl, Br, and I) perovskite nanocrystals by microwave irradiation. ACS Applied Materials & Interfaces, 2017, 9(49): 42919–42927
24. Liu H, Wu Z, Shao J, Yao D, Gao H, Liu Y, Yu W, Zhang H, Yang B. $CsPb_xMn_{1-x}Cl_3$ perovskite quantum dots with high Mn substitution ratio. ACS Nano, 2017, 11(2): 2239–2247
25. Leng M, Yang Y, Zeng K, Chen Z, Tan Z, Li S, Li J, Xu B, Li D, Hautzinger M P, et al. All-inorganic bismuth-based perovskite QDs with bright blue photoluminescence and excellent stability. Advanced Functional Materials, 2018, 28: 1704446-1–1704446-11
26. Jellicoe T C, Richter J M, Glass H F J, Tabachnyk M, Brady R, Dutton S E, Rao A, Friend R H, Credgington D, Greenham N C, Böhm M L. Synthesis and optical properties of lead-free cesium tin halide perovskite nanocrystals. Journal of the American Chemical Society, 2016, 138(9): 2941–2944
27. Woo H C, Choi J W, Shin J, Chin S H, Ann M H, Lee C L. Temperature-dependent photoluminescence of $CH_3NH_3PbBr_3$ perovskite quantum dots and bulk counterparts. Journal of Physical Chemistry Letters, 2018, 9(14): 4066–4074

28. Wang Y, Yang Y, Wang P, Bai X. Concentration- and temperature-dependent photoluminescence of $CsPbBr_3$ perovskite QDs. Optik (Stuttgart), 2017, 139: 56–60
29. Zhang J, Ma S, Fang H, Xu B, Sun H, Im C, Tian W. Insights into the origin of aggregation enhanced emission of 9,10-distyrylanthracene derivatives. Materials Chemistry Frontiers, 2017, 1(7): 1422–1429
30. Im C, Lupton J M, Schouwink P, Heun S, Becker H, Bässler H. Fluorescence dynamics of phenyl-substituted polyphenylenevinylene–trinitrofluorenone blend systems. Journal of Chemical Physics, 2002, 117(3): 1395–1402
31. Song J, Lee Y, Jin B, An J, Park H, Park H, Lee M, Im C. Connecting charge transfer kinetics to device parameters of a narrow-bandgap polymer-based solar cell. Physical Chemistry Chemical Physics, 2016, 18(38): 26550–26561
32. Hertel D, Romanovskii Y V, Schweitzer B, Scherf U, Bassler H. The origin of the delayed emission in films of a ladder-type poly (para-phenylene). Synthetic Metals, 2001, 116(1-3): 139–143